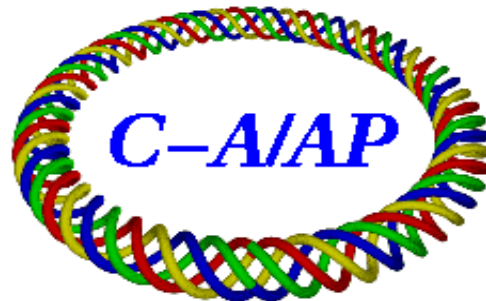


Dose/Sensitivity in Proton Computed Tomography

T. Satogata*, H.F.-W. Sadrozinski†, *Member, IEEE*, A. Dilmanian*, S. Peggs*, and A. Ruggiero*

*Brookhaven National Laboratory, Upton NY 11973

†Santa Cruz Institute for Particle Physics, Santa Cruz CA 95046



**Collider-Accelerator Department
Brookhaven National Laboratory
Upton, NY 11973**

Dose/Sensitivity in Proton Computed Tomography

T. Satogata*, H.F.-W. Sadrozinski[†] *Member, IEEE*, A. Dilmanian*, S. Peggs*, and A. Ruggiero*

* Brookhaven National Laboratory, Upton NY 11973

[†] Santa Cruz Institute for Particle Physics, Santa Cruz CA 95046

Abstract—Proton therapy has become an established form of cancer treatment, but dose calculations and treatment planning are routinely performed based on X-ray computed tomography (XRCT), which requires a conversion to proton stopping power. A more appropriate method to directly measure stopping power and dose is proton computed tomography (pCT), where high-energy protons are measured after traversing completely through the patient. Proton radiographs and pCT have historically been limited by blurring due to multiple scattering. However, proton-by-proton track reconstruction techniques, measuring entry positions and exit positions and energies of each scanning proton, promise to greatly improve the spatial resolution of proton radiographs. We use simplified physical models of proton transport (including Bethe-Bloch energy loss, energy straggling, and multiple Coulomb scattering) in the 0-300 MeV energy range of interest to analytically quantify the tradeoffs and scaling between dose, spatial resolution, density resolution, and scanning voxel size. Monte Carlo results and comparisons to this scaling are generated with a small “fast” Monte Carlo code specifically written for proton transport and pCT (pint).

I. INTRODUCTION

Proton-by-proton data recording is now becoming available at the accuracy and high rates necessary for proton computed tomography (pCT), thanks to technology transfer from high energy and nuclear physics experiments. The exit energy (or range) of individual protons can now be recorded, as well as their entrance and exit transverse displacements and angles, for example with the use of segmented calorimeters and silicon strip detectors. Proton-by-proton track reconstruction techniques promise to greatly increase the spatial resolution of proton radiographs, overcoming the multiple scattering problems that, in the past, have unacceptably blurred conventional radiographs. When a set of proton radiographs are taken from many angles, proton Computed Tomography can be performed in similar fashion to X-ray CT (XRCT), or proton emission tomography (PET), even though the proton trajectories tend not to be straight.

A prototype proton-by-proton “camera” has been installed on the PSI proton therapy gantry, and early operational performance has been reported, albeit without track reconstruction [1]. For example, Schneider and Pedroni [2] show radiographic projections produced by plotting the *average exit range* of protons, versus the transverse x and y coordinates measured in the entry plane. They also show “edge enhanced” images taken with the same data, when the *RMS exit range variation*

is plotted versus entrance x and y – making use of the multiple scattering phenomenon and proton range uncertainties [3].

While many imaging techniques can be envisaged, two particular methods are selected here, to quantify the relationship between dose, spatial resolution, and density resolution, in the idealized case of a perfect detection system. They are:

- 1) Average transmission method: Statistics are accumulated for each of a bundle of (not necessarily straight) proton trajectories through the object being imaged. The fraction of protons that is transmitted is measured as the “transmission” efficiency for each trajectory. This method is very similar to XRCT, so that it is relatively easy to compare XRCT and pCT doses in simulation. This has already been performed, preliminarily, by Satogata and Dilmanian et al. [4]
- 2) Average energy loss method: Again, statistics are accumulated for a bundle of trajectories, but in this method the quantity of interest is the average energy loss through each trajectory.

In all cases the best spatial resolution will only be obtained by using the best possible individual track reconstruction techniques, down to a fundamental limit defined by the physical phenomenon of multiple Coulomb scattering. It does not make sense to consider a bundle of proton trajectories with a transverse extent smaller than this physical limit.

The minimum transverse resolution through track reconstruction is considered briefly, below, in the section entitled “multiple scattering”. However, the spirit of this paper is that the *track reconstruction* problem is orthogonal to the *dose versus sensitivity* problem – so long as it is implicitly assumed that the spatial accuracy of track reconstruction is known, and that no attempt is made to exceed it.

II. SIMPLIFIED PHYSICAL MODEL

A. Linear energy transfer, range, and dose

The average rate of loss of energy (or *Linear Energy Transfer*, LET) for a single proton of instantaneous kinetic energy K , passing through water, is well-approximated by

$$\left| \frac{dK}{d\lambda} \right| [\text{MeV}/(\text{g}/\text{cm}^2)] \approx \frac{1}{0.098k + 0.0277} \quad (1)$$

in the energy range of medical interest, $0 < K[\text{MeV}] < 300$, with $k \equiv K/100$ [MeV]. The dimensions of λ are $[\text{g}/\text{cm}^2]$, so that in passage through a thickness Δs [cm] of water of density $\rho = 1$ $[\text{g}/\text{cm}^3]$,

$$\Delta\lambda = \rho\Delta s \quad (2)$$

Work performed under the auspices of the US Department of Energy; author email satogata@bnl.gov

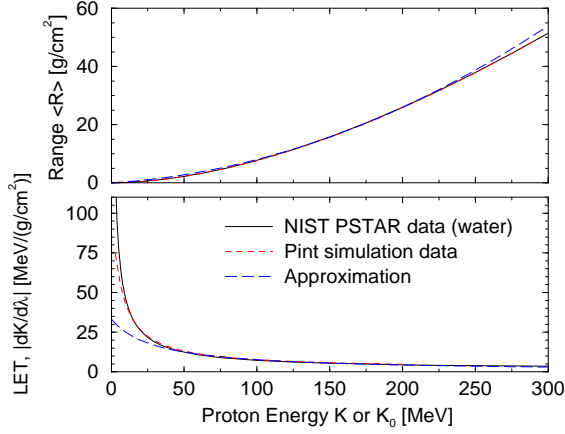


Fig. 1. Linear energy transfer $|dK/d\lambda|$ and mean range $\langle R \rangle$ for protons in water, versus local kinetic energy K or initial kinetic energy K_0 . Data are shown for NIST PSTAR reference data, pint Monte Carlo simulation, and the approximations of Eqs. 1 and 3.

This clearly illustrates Bragg peak behavior, in which most of the proton energy (and dose) is delivered just before it stops.

The average range $\langle R \rangle$ [g/cm²] of a proton of incident kinetic energy K [MeV] in water is approximately

$$\langle R \rangle \approx 4.90k^2 + 2.77k. \quad (3)$$

Eqns. 1 and 3 are related, since

$$\frac{d\langle R \rangle}{dK} = \left| \frac{dK}{d\lambda} \right|^{-1} \quad (4)$$

when the instantaneous energy is the maximum $K = K_0$, and λ is associated with the range $\langle R \rangle$. For example, a 200 MeV proton has an LET of about 4.47 [MeV/(g/cm²)], increasing dramatically just before it stops at the end of its mean range of about 26 g/cm² in water. This is illustrated in Fig. 1. Note that higher-order approximations can be applied to improve the low-energy behavior of the LET fit, Eqn. 1.

The dose in Grays is the energy deposition per unit mass, measured locally in Joules per kilogram. Thus, the average dose due to N protons passing through the face of a square pixel of size a is

$$D \equiv \frac{N}{\rho a^2 \Delta s} \left| \frac{dK}{d\lambda} \right| \rho \Delta s = \frac{N}{a^2} \left| \frac{dK}{d\lambda} \right| \quad (5)$$

or, more conveniently,

$$D[\text{Gy}] = 1.6 \times 10^{-10} \frac{N}{a^2[\text{cm}^2]} \left| \frac{dK}{d\lambda} \right| [\text{MeV}/(\text{g}/\text{cm}^2)] \quad (6)$$

For example, a single 200 MeV proton passing through a square pixel (or a cubic voxel) of size 0.1 cm delivers an average dose of about 7.2×10^{-8} Gy.

B. Straggling

The rate of energy loss of protons due to collisions with atomic electrons is a statistical process. Hence it is also necessary to consider “straggling”, the accumulation of an RMS

spread in energy loss and range, in addition to the average quantities considered above.

A proton beam passing through a material thickness $\Delta\lambda$ acquires an additional mean square energy spread of

$$\Delta\sigma_K^2 = 0.6 \frac{Z}{A} (m_e c^2)^2 \gamma \left(1 - \frac{\beta^2}{2} \right) \Delta\lambda \quad (7)$$

where m_e is the rest mass of an electron, Z and A are the atomic number and weight of the (pure) element being traversed, and β and γ are relativistic factors [5]. The growth rate is constant to a very good approximation in the medical energy range of interest, so that for water

$$\sigma_K^2 [\text{MeV}^2] \approx 0.089\lambda [\text{g}/\text{cm}^2] \quad (8)$$

By the time it reaches the Bragg peak, when $\lambda \approx \langle R \rangle$ just before stopping, a monochromatic beam has acquired a *total* RMS energy “straggle” of

$$\sigma_{KT} [\text{MeV}] = 0.30 \sqrt{\langle R \rangle [\text{g}/\text{cm}^2]} \quad (9)$$

This corresponds to an RMS range spread of

$$\sigma_R = \frac{d\langle R \rangle}{dK} \sigma_{KT} \quad (10)$$

or approximately

$$\sigma_R [\text{g}/\text{cm}^2] \approx 0.30 (.098k + .028) (4.90k^2 + 2.77k)^{1/2}. \quad (11)$$

For example, a monochromatic 200 MeV proton beam has an RMS kinetic energy spread of about 1.53 MeV at the end of its range of 26 g/cm², and an RMS range spread of about 0.34 g/cm² (0.34 cm in water).

C. Multiple Coulomb scattering

Independently of the energy loss process, the incident proton beam acquires an increasing transverse angular spread, and hence also transverse size, through the process of multiple Coulomb scattering (MCS). Even if the incoming beam has zero size and zero angular spread (zero emittance), the transverse size of the beam soon becomes significant. Fig. 2 shows, for example, that a 200 MeV beam acquires an RMS transverse size of 0.65 cm by the end of its range in water. The spatial resolution of the radiographic image is defined by the RMS size of the beam on exit, if proton-by-proton track reconstruction is not possible, or is not performed. Typically this is a few millimeters, unacceptably large in comparison with the sub-millimeter resolution possible with XRCT, MRI, or even with PET imaging. This is the physical root cause of the poor reputation that proton radiography has historically acquired, due to the inevitable blurring in simple transmission images.

However, the acquisition of proton-by-proton displacements and angles at entry and exit means that the internal trajectory of each proton is known in a statistical sense at the sub-millimeter level, in typical cases. This is calculated analytically in [6], [7] and illustrated in Fig. 3, where 200 MeV protons enter with zero displacement and zero angle, but exit with at different displacements measured by a single detector layer with a crude

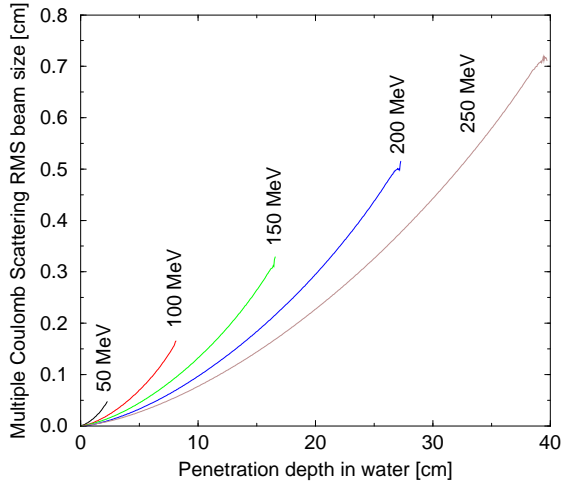


Fig. 2. Transverse proton beam size (due to MCS) versus depth in water for various energy incident protons, as calculated by pint Monte Carlo.

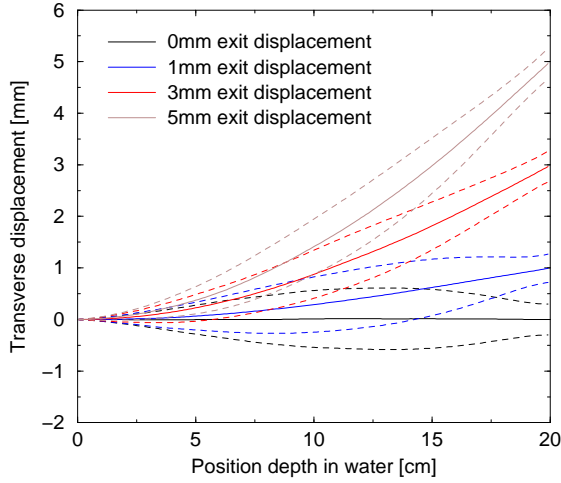


Fig. 3. Illustration of most likely paths and 1σ RMS envelopes, simulated for 200 MeV protons by pint Monte Carlo. The entrance position and angle are assumed known to sub-mm accuracy, and the exit displacement is assumed known to a 1 mm detector resolution.

resolution of 1 mm. The displacement angle is not measured. The solid lines indicate the most probable internal trajectory for each proton, with the dashed lines representing the one sigma statistical certainty. In the simple case of a water phantom, it is possible to answer these questions analytically [?]. Even with a crude exit displacement measurement, and no exit angle measurement, the internal trajectory is known to sub-millimeter accuracy.

If the exit angle is also measured, the most likely path envelope is further constrained as shown in Fig. 4. Clearly there is a limiting case even when exit angle and position are known to perfect accuracy. However, with realistic proton measurement resolutions the one-sigma proton envelope can be reduced to below 0.5 mm. We suggest that these Monte-Carlo simulations may be used as backprojection kernels for pCT reconstruction.

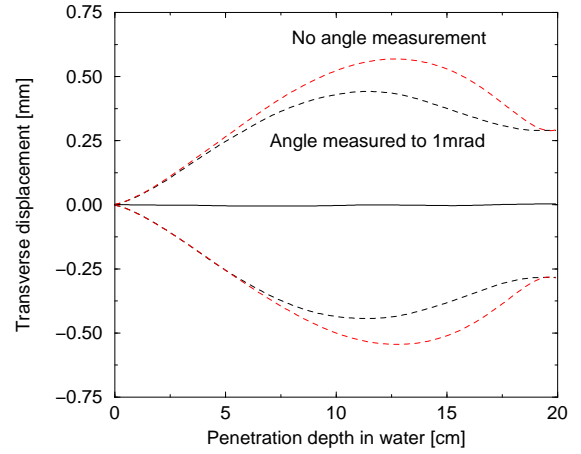


Fig. 4. A comparison of most likely paths and 1σ RMS envelopes, simulated for 200 MeV protons by pint Monte Carlo, with no knowledge of the exit proton angle and with exit proton angle known to 1 mrad. Exit angle constraints improve the most likely path uncertainty by up to 40%.

III. AVERAGE TRANSMISSION OBSERVATION

Fig. 5 illustrates the *average transmission* method suggested by Satogata and Dilmanian [4], in which the energy of the incoming beam and the profile of the bowtie filter are adjusted so that the Bragg peak falls at the distal edge of the bowtie, simultaneously minimizing the dose to the patient while maximizing the measurement sensitivity. The total straight line linear density, given by

$$\lambda(x, y) = \int_A^B \rho(s) ds + \int_C^D \rho_{\text{bowtie}} ds \quad (12)$$

is a function of the transverse co-ordinates x and y at entrance. The fraction of the proton beam transmitted is a function of λ and the initial kinetic energy K_0 , $T = T(\lambda, K_0)$ as sketched in Fig. 6. Transmission is measured for each square *entrance* pixel of size a as

$$T_{\text{meas}} = \frac{N_{\text{out}}}{N} \quad (13)$$

where N protons enter each pixel, but only N_{out} exit (anywhere) from the bowtie, into a downstream counter. The accuracy with which T_{meas} represents T increases with the number of incident protons N as follows

$$T_{\text{meas}} = T \pm \frac{\sqrt{N_{\text{out}}}}{N} = T \pm \sqrt{\frac{T}{N}} \quad (14)$$

How many incident protons are needed to resolve a fractional density variation of $\delta \equiv \Delta\rho/\rho_0$ in a cubic voxel of size a ? To detect such a variation the transmission T must be measured with an accuracy

$$\Delta T = \frac{dT}{d\lambda} \Delta\lambda = \frac{dT}{d\lambda} \rho_0 a \delta \quad (15)$$

Eqn. 14 shows that approximately

$$N \simeq \frac{T}{\Delta T^2} \quad (16)$$

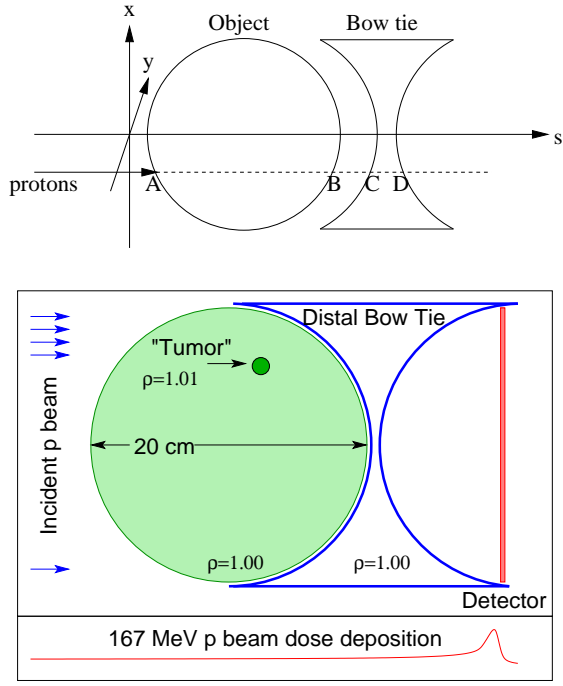


Fig. 5. Schematic layout of object being radiographed, plus compensating ‘Bow tie’. The simple phantom shown at the bottom has been used in preliminary reconstruction simulations. [4]

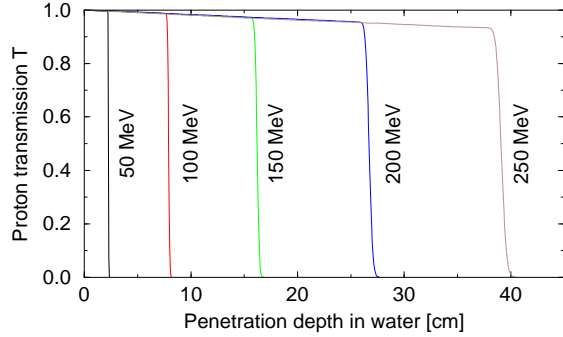


Fig. 6. Sketch of the transmission T versus linear density λ , for different incident proton kinetic energy K . The constant-angle losses are from inelastic nuclear scattering.

incident protons are needed per pixel. This leads to the principal result that for a single radiographic projection

$$N\delta^2 a^2 = \frac{T}{(dT/d\lambda)^2 \rho_0^2} \quad (17)$$

Note that this expression can readily be applied to photons in X-ray imaging.

A. The optimum dose-sensitivity solution

Fig. 6 suggests that the right hand side of Eqn. 17 is minimized (for the highest sensitivity δ and the least dose D on the left hand side) by adjusting the incident kinetic energy K_0 to maximize the transmission slope $dT/d\lambda$. The range distribution $\phi(R)$ has a significant Landau tail. Nonetheless, for current

purposes it is convenient to assume that the range distribution is Gaussian

$$\phi(R) = \frac{1}{\sqrt{2\pi}\sigma_R} \exp\left(-\frac{(R - \langle R \rangle)^2}{2\sigma_R^2}\right) \quad (18)$$

In that case, if nuclear losses are ignored, then

$$\frac{dT}{d\lambda} = -\phi(\lambda) \quad (19)$$

and the steepest transmission slope, which occurs when $\lambda = \langle R \rangle$ and $T = 0.5$, is given by

$$\left|\frac{dT}{d\lambda}\right|_{\max} = \frac{1}{\sqrt{2\pi}\sigma_R} \quad (20)$$

Thus, when the initial kinetic energy K_0 is tuned so that half of the protons penetrate the object and the bow tie, then according to Eqn. 17

$$N\delta^2 a^2 = \frac{\pi\sigma_R^2}{\rho_0^2} \quad (21)$$

The local dose D that is delivered by this flux of protons depends on the local energy K , as well as the initial energy K_0 , since by invoking Eqn. 5

$$D\delta^2 a^4 = \frac{\pi\sigma_R^2}{\rho_0^2} \left|\frac{dK}{d\lambda}\right| \quad (22)$$

In particular, when $K = K_0$ at the surface of the patient, then applying Eqns. 4, 9, and 10 gives

$$D\delta^2 a^4 = \frac{0.089\pi}{\rho_0^2} \langle R \rangle \frac{d\langle R \rangle}{dK} \quad (23)$$

Substituting Eqns. 1 and 11 gives the convenient approximations

$$N\delta^2 a^2 [\text{cm}^2] \approx \frac{0.28}{\rho_0^2} (4.9k^2 + 2.8k)(0.10k + 0.03)^2 \quad (24)$$

and

$$Da^4\delta^2 [\text{Gy cm}^4] \approx \frac{4.5 \times 10^{-11}}{\rho_0^2} (4.9k^2 + 2.8k)(0.10k + 0.03) \quad (25)$$

where, as usual, $k \equiv K/100$ [MeV], and $\rho_0 \approx 1.0$ g/cm³. For example, consider a 200 MeV proton beam being used in water to detect a $\delta = 0.01$ density fluctuation in voxels of size $a = 0.1$ cm. In this case $N\delta^2 a^2 \approx 0.37$, $N = 370,000$ protons are needed for every pixel, and the surface dose (when $K = 200$ MeV) is $D = 26$ mGy.

Eqns. 22 and 25 record the dose for a single radiograph projection. In a computed tomograph over a field of view of width W , approximately

$$M = \frac{W}{a} \quad (26)$$

angles are required. Thus, the total CT dose scales like

$$D \sim \frac{W}{a^5\delta^2} \quad (27)$$

with a very strong fifth power dependence on a , the voxel size.

IV. PROTON-BY-PROTON ENERGY LOSS OBSERVATION

Instead of simply counting the fraction of protons that exit, in a transmission measurement, it is now assumed that *the energy of each individual proton is measured*, and that the goal is to reconstruct the density of each voxel by accurately recording the energy loss there. A perfect energy detector (for example a calorimeter) is assumed, so that the dose-sensitivity relation derived below is a fundamental limit. As before, it is assumed that the track reconstruction is accurate enough that it is known through which voxels each proton passes.

The total energy deposited when N protons pass through a basis trajectory of square dimension a is

$$\Delta K = N \int \left| \frac{dK}{d\lambda} \right| \rho(s) ds \pm N^{1/2} \sigma_{KT} \quad (28)$$

where the second term represents the measurement error that is present, due to the *total* straggling fluctuations,

$$\sigma_{KT} = \left(\int \frac{d\sigma_K^2}{d\lambda} \rho(s) ds \right)^{1/2} \quad (29)$$

even for a perfect calorimeter. Clearly, the error in the measurement of the *average* energy loss per proton ($\Delta K/N$) decreases statistically like $1/\sqrt{N}$. This is why more protons are needed to resolve smaller fluctuations in density, in a single radiograph projection. For example, if the density of a single voxel in this trajectory deviates in density by $\delta = \Delta\rho/\rho_0$, then the average total energy loss changes by

$$\delta\Delta K = N \left| \frac{dK}{d\lambda} \right| \delta\rho_0 a \quad (30)$$

where $|dK/d\lambda|$ must be evaluated at the instantaneous kinetic energy K corresponding to that particular voxel. Thus the condition for detection of this density deviation is just

$$N \left| \frac{dK}{d\lambda} \right| \delta\rho_0 a > N^{1/2} \sigma_{KT} \quad (31)$$

or, leaving just the intensity and sensitivity terms on the left hand side, the detection threshold is at

$$N\delta^2 a^2 = \frac{1}{\rho_0^2} \frac{\sigma_{KT}^2}{|dK/d\lambda|^2} \quad (32)$$

This is converted to a dose-sensitivity relationship by invoking Eqn. 5 to give

$$D\delta^2 a^4 = \frac{1}{\rho_0^2} \frac{\sigma_{KT}^2}{|dK/d\lambda|^2} \quad (33)$$

In a more convenient form for quantification,

$$N\delta^2 a^2 [\text{cm}^2] \approx \frac{0.089\lambda}{\rho_0^2} (.10k + .03)^2 \quad (34)$$

and

$$D\delta^2 a^4 [\text{Gycm}^4] \approx \frac{1.4 \times 10^{-11}\lambda}{\rho_0^2} (.10k + .03) \quad (35)$$

where λ is the total thickness of the patient, the instantaneous energy $k \equiv K/100$ is, as ever, measured in MeV, and $\rho_0 \approx 1.0 \text{ g/cm}^3$. Consider again the *surface* dose delivered

by a 200 MeV proton beam being used in water to detect a $\delta = 0.01$ density fluctuation in voxels of size $a = 0.1 \text{ cm}$, but now with a thickness of $\lambda = 20 \text{ g/cm}^2$, and no bow tie filter. Since now $N\delta^2 \approx 0.094$, about 94,000 protons are needed to penetrate each pixel, and the local dose is about 6.6 mGy, per radiographic projection. Superficially, this is about half an order of magnitude less than the the dose received using the average transmission method. However, these results neglects the increased dose necessary due to imperfect energy measurement detectors, and due to other imperfections in both approaches.

These results, and the results from the average transmission method, show the same scaling with a , since with about W/a radiographic projections for each CT the total dose goes like

$$D \sim \frac{W}{a^5 \delta^2} \quad (36)$$

V. CONCLUSIONS

We have reviewed the relationships, scalings, and energy-appropriate approximations for pCT models. These include linear energy transfer, proton range, and dose (material energy deposition) from Bethe-Bloch energy losses, energy straggling, and multiple coulomb scattering. These approximations have been compared to a simple, fast Monte Carlo code pint, written by the author and used for simulations of pCT for detector and experiment development. Spatial track resolution of pCT is sub-millimeter when entrance and exit positions and angles are measured as accurately as possible. Scaling arguments have shown that dose D vary with voxel size a and required density resolution δ as $D \propto a^{-5}\delta^{-2}$, demonstrating a very strong dependence on voxel size. Further Monte Carlo work and reconstruction techniques, including most-likely envelope backprojection, are in development to demonstrate this scaling.

ACKNOWLEDGMENTS

We are very thankful to Joanne Beebe-Wang, Steve Hancock, Steve Kramer, David Williams, Jerome Liang, Klaus Mueller, Eros Pedroni, and Uwe Schneider for critical discussions during the construction of this paper.

REFERENCES

- [1] P. Pemler et al., *A Detector System for Proton Radiography on the Gantry of the Paul Scherrer Institute*, Nucl. Inst. and Meth. A **432**, pp. 483–495 (1999).
- [2] U. Schneider and E. Pedroni, *Proton Radiography as a Tool for Quality Control in Proton Radiography*, Med. Phys. **22** (1995) 4.
- [3] U. Schneider and A. Tourovsky, *Range-Uncertainty Imaging for Obtaining Dose Perturbations in Proton Therapy*, IEEE Trans. on Nuc. Sci. **45** (5) pp. 2309-2313 (1998)
- [4] T. Satogata et al., *Reduced Dose of Proton CT Compared to X-Ray CT in Tissue-Density Variation Sensitivity*, (Poster M10-204) 2002 IEEE NSS/MIC in Norfolk, VA, Nov. 2002.
- [5] D. Perkins, *Introduction to High Energy Physics*, 3rd ed., Harlow, England: Addison-Wesley, 1987, pp. 39–66.
- [6] U. Schneider, *Proton Radiography: A Tool For Quality Control in Proton Therapy*, Ph.D. Thesis, 1994, ETH Zurich.
- [7] D.C. Williams, *The Most Likely Path of an Energetic Charged Particle through a Uniform Medium*, SCIPP preprint 03/07.
- [8] U. Schneider and E. Pedroni, *Multiple Coulomb Scattering and Spatial Resolution in Proton Radiography*, Med. Phys. **21** (1994) 1657.